Noncovalent Porphyrin–Graphene Oxide Nanohybrids: The pH-Dependent Behavior

Gacka, E.; Lindner, A. A.; Mazurkiewicz-Pawlicka, M.; Malolepszy, A.; Stobiński, L.; Kubas, A.; Hug, G. L.; Marciniak, B.; Lewandowska-Andralojc, A.;

Originally published:

January 2019

Journal of Physical Chemistry C 123(2019), 3368

DOI: https://doi.org/10.1021/acs.jpcc.8b11374

Non-Covalent Porphyrin-Graphene Oxide Nanohybrids: the pH Dependent Behaviour

Ewelina Gacka,[a] Aleksandra Wojcik,[b] Marta Mazurkiewicz-Pawlicka,[c] Artur Malolepszy,[c] Leszek Stobiński,[c] Adam Kubas,[d] Gordon L. Hug,[e] *Bronislaw Marciniak,[a] Anna Lewandowska-Andralojc,*[*a]*

[a]Faculty of Chemistry, Adam Mickiewicz University, Umultowska 89b, 61-614, Poznan, Poland, alewand@amu.edu.pl

[b]Helmholtz-Zentrum Dresden-Rossendorf, Institute of Ion Beam Physics and Materials Research, Bautzner Landstraße 400, 01328 Dresden, Germany

[c]Faculty of Chemical and Process Engineering, Warsaw University of Technology, Warynskiego 1, 00-645 Warsaw, Poland

[d]Institute of Physical Chemistry, Polish Academy of Sciences, Kasprzaka 44/52, 01-224 Warsaw, Poland

[e]Radiation Laboratory, University of Notre Dame, Notre Dame, USA

ABSTRACT

Non-covalent nanohybrids between *meso*-(p-hydroxyphenyl)porphyrin (TPPH) and graphene oxide (GO) sheets were studied as a function of pH. The overall charge of the TPPH molecule changes between negative (-4), neutral and positive (+2) depending on the pH of the solution. Results of FTIR, thermogravimetric analysis (TGA), and elemental analysis confirm successful non-covalent functionalization of graphene oxide sheets with TPPH. We applied a number of methods to probe the ground state as well as the excited state interaction between the components of the new material. The experimental results were additionally supported by theoretical calculations that included optimizations of the ground state structures of TPPH and $TPPH^{2+}$ and its complexes with a molecular model of the GO. It was demonstrated that both TPPH and $TPPH^{2+}$ molecules can be assembled onto the surface of graphene oxide, but it was clearly shown that the stronger interaction with GO occurs for $TPPH^{2+}$. The stronger interaction in acidic environment can be rationalized by the electrostatic attraction between positively charged $TPPH^{2+}$ and negatively charged GO whereas the interaction between $TPPH^{4-}$ and GO at basic pH was largely suppressed. Our comprehensive analysis of the emission quenching led to the conclusion that it was solely attributed to static quenching of the porphyrin by GO. Surprisingly, fluorescence was not detected for the nanohybrid which indicates that a very fast deactivation process must take place. Ultrafast time-resolved transient absorption spectroscopy demonstrated that, although the singlet excited state lifetime of $TPPH^{2+}$ adsorbed on the GO sheets was decreased in the presence of the GO from 1.4 ns to 12 ps, no electron transfer products were detected. It is highly plausible that electron transfer takes place and is followed by fast back electron transfer.

Introduction

Graphene is an outstanding 2D material composed of sp^2-hybridized carbon atoms and is characterized by unique physical and chemical properties, e.g. excellent conductivity, large surface area, and zero band gap.[1-5] Graphene based nanomaterials have been extensively explored due to their potential applications, i.e. solar energy conversion, optoelectronic devices, catalysis and sensing.[6-11] However, as a consequence of strong π-π interactions between graphene sheets, it has a tendency to aggregate, which limits the extent of its applications. From a practical point of view graphene oxide (GO), which is a graphene derivative bearing various oxygen-derived functional groups (such as epoxy, hydroxyl, carbonyl and carboxyl), seems to be more appropriate for constructing graphene based functional materials.[12-13,35] Graphene oxide is usually synthesized by exfoliation of graphite through strong oxidization.[12, 14,35] Although the properties of graphene oxide remain inferior to those of pristine graphene, the decoration with numerous oxygen-containing groups at the basal planes of graphene sheets allows it to form stable aqueous suspensions. This is important for processing and for further derivatization. Thus, GO is a promising platform for the preparation of graphene-based nanomaterials that can find application in both fundamental research as well as in photocatalytic systems, optical devices or sensing.

One approach is to functionalize GO sheets with molecules that are photochemically active. The concept of dye/graphene materials is that graphene plays the role of electron mediator/transporter and supporting matrix for the attached sensitizer, which in turn broadens the light absorption of the nanohybrid into the visible range. The synthesis of dye/graphene oxide composites can be achieved via its covalent or non-covalent functionalization.[8] Covalently functionalized graphene, owing to its sophisticated and low yield synthesis, is limited in its application. The noncovalent strategy relies on molecular interactions, such as π–π stacking, hydrogen bonding, or charge

attraction between graphene and organic molecules. The great advantage of this approach is facile synthesis, i.e. it requires only mixing of a dye solution with a dispersion of graphene oxide.

Among a variety of organic dyes, porphyrins are well studied due to their excellent photoactive properties. Porphyrins are planar and electron rich aromatic molecules, characterized by remarkably high extinction coefficients in the visible region. These properties enabled their wide application as photosensitizers in artificial photosynthetic systems.[15] Therefore, porphyrins and graphene oxide represent promising candidates for fabrication of new nanohybrid materials. In the past few years, new porphyrin/graphene based materials were explored by a number of research groups.[6, 16-26] Wojcik et al described efficient non-covalent functionalization of reduced graphene oxide (RGO) with the cationic porphyrin TMPyP (5,10,15,20-tetra(1-methyl-4-pyridino) porphyrin tetra(p-toluenesulfonate). The authors confirmed by femtosecond transient absorption and photoelectrochemical measurements the occurrence of photoinduced electron transfer in TMPyP-RGO nanohybrids.[20] The Zhu group reported enhanced photocatalytic activity toward hydrogen generation in the system where the 5,10,15,20-tetrakis(4-(hydroxyl)phenyl) porphyrin (TPPH) molecules play the role of photosensitizer adsorbed on the surface of RGO sheets with Pt nanoparticles acting as a dispersed co-catalyst.[16] More recently Yuan et.al. presented a non-noble metal system for photocatalytic H_2 generation that combined Zn(II)-5,10,15,20-tetrakis(4-*N*-methylpyridyl)porphyrin and RGO with decorated MoS_2 as the catalyst.[17] Guo has shown that the zinc 5,10,15,20-tetra(4-pyridyl)-21H,23H-porphine nanostructures, assembled onto GO sheets via a surfactant assisted method, displayed photocatalytic activity for the degradation of rhodamine B.[27] It was also demonstrated that porphyrin/GO composites can be used as an optical probe for the detection of iron(III) ions. The novel sensor was constructed based on tetrakis(trimethylammoniophenyl)porphyrin and graphene oxide.[23] Although significant progress

has already been achieved in the field of dye/graphene nanohybrids, further efforts are still required for a knowledge-driven design of materials with desired properties. In the literature of porphyrin/graphene nanocomposites, what is still lacking are comprehensive studies that combine detailed steady-state spectroscopic and time-resolved measurements complemented with characterization of the morphology and structure of the graphene based hybrid materials.

In this work, we focused on *meso*-(p-hydroxyphenyl)porphyrin (TPPH) since it is a very important porphyrin widely used as a photosensitizer. [16, 28-30] There are already several reports on the non-covalent interactive affair between TPPH and graphene oxide or reduced graphene oxide, but none of these reports present the influence of the pH on the formation of the nanohybrids.[16, 25] Also, in previous work, the TPPH-nanohybrids' spectroscopic properties were studied mainly in ethanol whereas in this work we used EtOH-H_2O(1:2 v/v) which is advantageous in the view of future applications.

Herein, we describe the preparation of non-covalent nanohybrids between TPPH and graphene oxide sheets under acidic, neutral and basic pH. The interesting aspect attracting us to this noncovalent functionalization of GO is that the overall charge of the TPPH molecule changes between negative (-4), neutral and positive (+2) depending on the pH of the solution (Scheme 1). TPPH at neutral pH does not possess charge. However, protonation of the imino nitrogens increases the overall charge to +2. On the other hand, deprotonation of the -OH groups in the substituents at basic conditions introduces negative charge on TPPH.

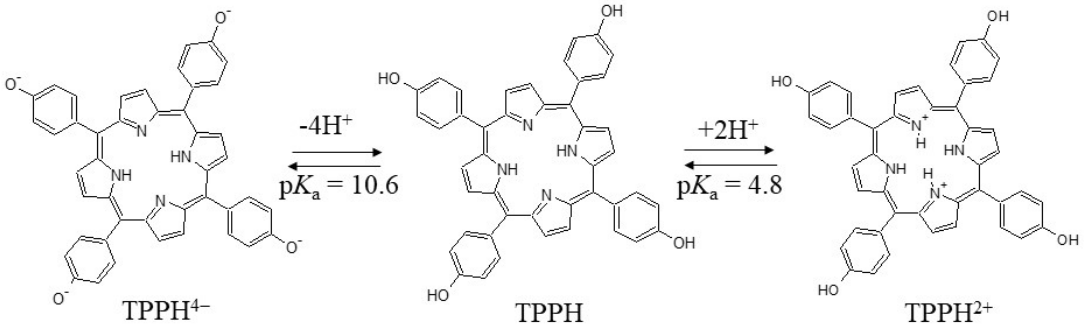

Scheme 1. Molecular structure and ionic equilibria of the 5,10,15,20-tetrakis(4-(hydroxy)-phenyl) porphyrin.

Aqueous suspensions of GO sheets are negatively charged, thus it was expected that the strength of the interaction between the GO and the porphyrin molecule can be modulated by changing the pH. At low pH the electrostatic interaction between GO and $TPPH^{2+}$ should favor nanohybrid formation. In contrast, at basic pH, where the porphyrin exists as an anion, $TPPH^{4-}$ adsorption onto GO sheets intuitively should to be largely suppressed. Herein, we report comprehensive studies into the interaction of TPPH with GO as a function of pH. The authors of the paper are aware of only one publication in which the interaction of porphyrin TMAP with GO was examined under two different pH values.[31]

It should also be pointed out that, in the vast majority of the reports on GO-based assemblies, the interaction of graphene with the dyes was marked only by fluorescence quenching of organic molecules and/or photocurrent measurements.[16, 32-34] The limited number of techniques applied so far does not allow for a clear determination of the quenching mechanism. Several possibilities should be taken into account and carefully analyzed for the interaction between the porphyrin and graphene, i.e. electron transfer, energy transfer, static quenching. In addition the use of graphene oxide, which is a unique material without a well-defined chemical formula, presents challenges for the quantitative analysis of the emission data which need to be performed with special attention.

The presence of the GO may distort the emission data due to light absorption and scattering. Moreover, any comparative emission studies require matching absorbances at the excitation wavelength. Thus, our contribution to the work in this area is to provide precise spectroscopic measurements and data analyses, that could be helpful for other scientists.

Results of FTIR, elemental analysis and thermogravimetric analysis (TGA) proved that there was efficient non-covalent functionalization of graphene oxide sheets with TPPH. At acidic pH the interaction of $TPPH^{2+}$ with GO was indeed found to be stronger, and it was largely suppressed at basic pH. We employed a number of methods (UV-vis absorption, steady-state and time resolved fluorescence, nanosecond and femtosecond transient absorption measurements) to investigate the ground state as well as the excited state interaction between the components of the new material. The collected data pointed to a fast photoinduced electron transfer process from the singlet excited state of the porphyrin to the GO moiety. The experimental results were additionally supported by theoretical calculations that included the optimization of the ground state structure of TPPH and $TPPH^{2+}$ and its complexes with GO along with interaction energy calculations. These comprehensive studies can provide invaluable information that can serve as guidance for fabrication of energy conversion devices.

Experimental

Materials

5,10,15,20-tetrakis(4-(hydroxyl)-phenyl) porphyrin (TPPH) and 5,10,15,20-tetrakis(4-methoxyphenyl)porphyrin (TPPOMe) were purchased from Sigma Aldrich, and graphite powder was purchased from Acros Organics. Ethanol (HPLC grade) was bought from J.T. Baker. Solutions were prepared with millipore distilled water (18 MΩ cm).

Preparation of the GO

Graphene oxide was prepared by oxidizing graphite powder using a modified Hummer's method.[35] In short, 10 g of graphite powder were mixed with 230 ml of concentrated (98 wt%) sulfuric acid at a temperature below 10 °C. Subsequently, 4.7 g of sodium nitrate and 30 g of potassium permanganate were carefully added to the mixture while the temperature was kept below 10 °C. Then the mixture was carefully heated to 30 °C and stirred for two hours. The next step involved adding 100 ml of deionized water. The slurry temperature was raised to 100 °C. In the final step, 10 ml of hydrogen peroxide was added to the mixture. The obtained dark yellow suspension was thoroughly washed and filtrated with deionized water until the pH of the filtrate reached 6.5.

Preparation of the TPPH-GO hybrid

90 ml of TPPH solution (1.5×10^{-5} M) (EtOH-H_2O, 1:2 v/v) was mixed with 6.4 ml of aqueous GO suspension (3 mg ml^{-1}), and the pH of the mixture was adjusted to 3.0 by the addition of HCl aqueous solution. The mixture was then stirred at room temperature for 2 h, resulting in TPPH−GO hybrids. Subsequently the obtained suspension was centrifuged at 12000 rpm (14986 rcf) for 90 minutes. The obtained supernatant was light yellow, and the precipitate was dark brown. TPPH-GO powder was obtained by drying the wet precipitate in an oven for 20 h at 65ºC.

Apparatus

UV-vis absorption spectra were recorded using a two-beam spectrometer Cary 100 UV-Vis scanning from 200 to 800 nm with 1 nm increments. Quartz cells with 10 mm optical lengths were used. Fluorescence spectra were taken on a LS 50B spectrofluorometer (Perkin Elmer) with excitation and emission slits of 10 nm. Emission spectra were measured on solutions with absorbances at the excitation wavelength not higher than 0.1. Emission was scanned between 500

and 800 nm for all samples. Emission lifetimes were measured using a FluoTime300 spectrometer (PicoQuant) operating in the time-correlated single photon counting mode (TCSPC). A light-scattering Ludox solution (colloidal silica) was used to obtain the instrument response function (prompt). Quartz cells with 10 mm optical length were used for all measurements.

Femtosecond transient absorption measurements were conducted using the Solstice Ti:sapphire regenerative amplifier from Spectra Physics and an optical detection system provided by Ultrafast Systems (Helios). The source for the pump and probe pulses was the fundamental emission at 800 nm. The fundamental output was split into two beams: a pump (95%) and a probe (5%). The pump beam was directed through the TOPAS-Prime automated optical parametric amplifier from the Spectra Physics to obtain the desired excitation wavelength in the range 290-2600 nm. The probe beam was directed to the Helios: a CCD-based pump-probe TA spectrometer from Ultrafast Systems LLC with an optical delay line allowing delay between the pump and probe up to 3.2 ns. For the detection of the transients, a white light continuum was used, which was generated from the 5% of the fundamental beam by passing it through a sapphire or calcium fluoride crystal.

The setup for the nanosecond laser flash photolysis (LFP) experiments and the data acquisition system have been previously described in detail.[36] LFP experiments employed a Nd:YAG laser (355 nm, 5 mJ, 7–9 ns) for excitation. Transient decays were recorded at individual wavelengths by the step-scan method with a step distance of 10 nm in the range of 300 to 800 nm as the mean of 10 pulses. Solutions for LFP were deoxygenated with high-purity argon for 15 min prior to the measurements. Experiments were performed in rectangular quartz cells (1 cm × 1 cm).

Thermal properties of the samples were characterized by a thermogravimetric analysis (Mettler Toledo TGA/DSC3+). The samples' measurements were carried out under an argon atmosphere from room temperature to 1200 °C at 10 °C min^{-1}. ATR-FTIR spectra were collected on a FTIR

Spectrometer Nicolet iS10 (Thermo Scientific) (range 400-4000 cm^{-1}). Elemental analysis measurements were obtained by using a Thermo Scientific Flash 2000 CHNS/O analyzer.

Computational methods

Calculations presented in the manuscript were carried out within the density functional theory (DFT) as implemented in the ORCA 4.0.1 suite of programs.[37-38] We used the semi-local BP86 functional[39-40] for geometry optimizations and the hybrid BHLYP functional[41] to characterize the electronic structure of the examined molecular assemblies. The latter is superior in cases where significant charge-transfer is expected and thus provides better ordering of key frontier orbitals.[42] The triple-ζ quality def2-TZVP basis set[43] was employed throughout the study. The density functionals were supplemented with two *a posteriori* corrections: (i) D3BJ[44-45] that accounts for deficiencies in mid- and long-range exchange-correlation potential that is important for a proper description of van der Waals interactions and (ii) gCP[46] that decreases the basis set superposition error in a pair-wise manner. Coulomb integrals were evaluated with the RI approximation using special def2-TZVP/J fitting basis.[47] In the case of the BHLYP functional, we employed the COSX approximation[48] for fast semi-numerical calculations of exchange integrals. The obtained structures were subject to numerical second derivative calculations and possessed only positive eigenvalues. Graphene oxide was simulated as a 111 atom neutral structure that possess all relevant functional groups such as epoxides, carbonyl groups or hydroxyl groups. It essentially resembles the model proposed by He and co-workers[49] and has an extended 2D structure in the nano-sized regime (ca. 1.7 x 1.7 nm). Cartesian coordinates of all structures relevant to this study are provided in the Supplementary Information.

Results and discussion

Preparation and Characterization of the TPPH–GO Hybrid Nanocomposite

A TPPH solution was mixed with an aqueous suspension of GO and subsequently acidified to pH 3, yielding a dark brown suspension subjected further to centrifugation (Scheme 2). Fig. 1 shows the UV-vis spectra of the suspension before and after centrifuging.

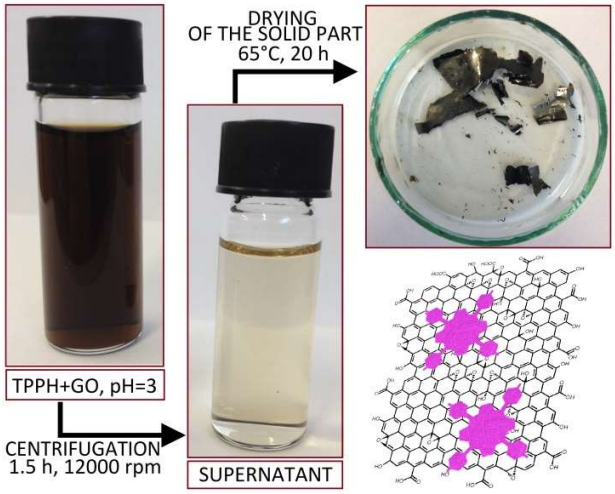

Scheme 2. Schematic overview of the TPPH─GO nanohybrid formation.

Based on the minor peak attributed to the porphyrin detected in the suspension, it was estimated that ca. 90% of the nanohybrid was successfully isolated as the precipitate. Interestingly, suspending again the precipitate resulted in the reconstruction of the UV-vis spectra of the nanohybrid. When the analogous process of nanohybrid formation was performed under neutral pH, a peak at 418 nm, attributed to free TPPH, was found in the UV-vis spectra of the supernatant after centrifugation (Figure S1). This indicates that the interaction between TPPH and GO is rather weak and can be partially destroyed during the centrifuging process. A similar experiment was carried out under basic conditions (pH 11.5), where a weaker interaction between $TPPH^{4-}$ and GO sheets was expected, due to repulsive interactions. Indeed, the supernatant at pH 11.5 contained all of the dye that was used in the experiment, indicating the precipitation of GO without any

porphyrin adsorbed on it (Figure S2). This proves that under basic pH the formation of the nanohybrids was largely suppressed.

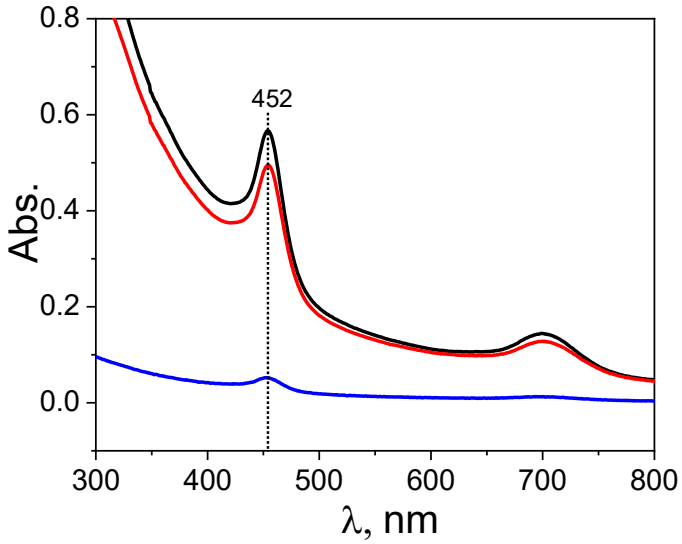

Figure 1. Absorption spectra of $TPPH^{2+}$ with the addition of GO suspension (black line), spectrum of the supernatant after centrifuging (blue line), suspended precipitate after centrifugation (red line).

The confirmation for the successful functionalization of GO with porphyrin was derived from thermogravimetric analysis. Figure 2 displays the TGA curves of GO, TPPH and TPPH-GO which were registered in an argon atmosphere from room temperature to 900 °C. The mass loss of about 16% from room temperature to 180 °C for GO can be ascribed to the loss of adsorbed water. The mass loss of about 24% at 215 °C was related to the pyrolysis of unstable oxygen-functional groups. Thermal decomposition of GO was completed at 875 °C. In the case of TPPH-GO, the thermal properties are very similar to GO up to 500 °C. Interestingly, above 500 °C the presence of TPPH in the nanohybrid enhanced the thermal stability of the GO. The presence of only 3.3% wt. of TPPH in the nanohybrid (based on the elemental analysis, *vide infra*) was sufficient to significantly increase the thermal stability of the material.

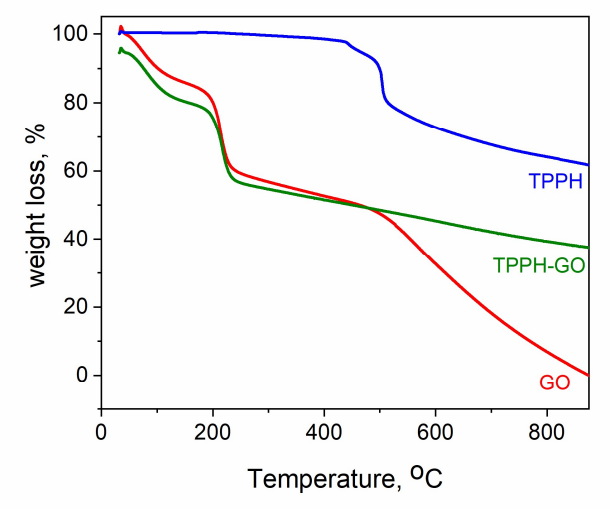

Figure 2. The thermogravimetric analysis (TGA) curves of the GO (red), TPPH (blue) and TPPH-GO nanohybrid (green).

Figure 3 displays the FTIR spectra of GO along with the TPPH-GO nanohybrid and TPPH for the purpose of comparison. The FTIR spectrum of GO shows several bands attributed to oxygen functionalization (Figure 3). The broad peak that occurs around 3000 cm^{-1} can be attributed to the stretching vibrations of the C–OH stretching vibrations of a hydroxyl group. Other peaks can be detected at: 1719 cm^{-1} (stretching vibrations of the C=O bonds in carboxylic and carbonyl groups), 1590 cm^{-1} (skeletal vibrations of the C=C bonds in non-oxidized graphite which is presumably overlapped with vibration of the O-H bonds in the water molecules, which is present in the sample), 1225 cm^{-1} (stretching vibrations of the C-O bonds) and 1040 cm^{-1} (stretching vibrations of the C-O-C bonds in the epoxy groups). In the FTIR spectrum of TPPH, the absorption band with strong intensity located at 3496 cm^{-1} is assigned to the O-H stretching vibration, and the absorptions at 3398 and 966 cm^{-1} are attributed to stretching and bending vibrations of N-H and C-N, respectively, which are characteristic absorptions of the porphyrin free base. The bands in the range 1500-1600 cm^{-1} are due to the stretching vibration of C=C in the benzene aromatic ring. The

bands at 1169 cm^{-1} can be ascribed to stretching vibrations of the C-O of phenols. Bands at 812 and 728 cm^{-1} are related to C-H bond bending vibrations of para-substituted phenyls. The TPPH-GO spectrum strongly resembles the spectrum of the pure graphene oxide. However the FTIR spectrum of the TPPH-GO nanohybrid additionally exhibited signals characteristic for the fingerprint region of the porphyrin, among others at 848 cm^{-1} and 1169 cm^{-1}, which were not present in the spectrum of GO itself. All of these bands clearly confirm that the porphyrin was adsorbed onto the GO surface and that the interaction between the moieties is strong.

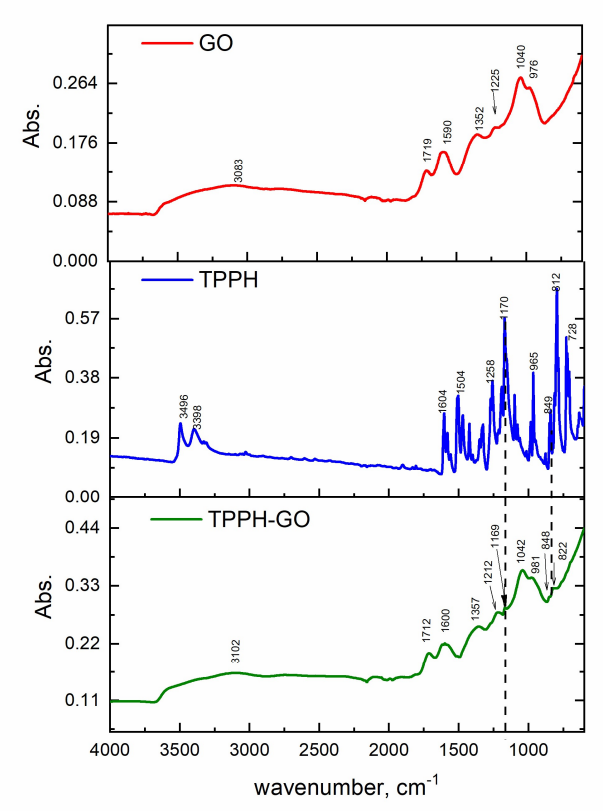

Figure 3. The FTIR spectra of the TPPH, GO and the TPPH-GO nanohybrid.

Elemental analysis provides further confirmation of the effective adsorption of the TPPH molecules to the graphene oxide sheets (Table 1). As can be seen in Table 1, the carbon/oxygen ratio in GO was roughly 1.0 which indicates that the GO used in this study was a highly oxidized

graphene material. Of particular note is the low level of sulfur (<0.54%). It has been shown in the literature, that graphene oxide synthesized via Hummers' method, even after extensive washing, tends to have detectable amounts of sulfur.[50] In the TPPH-GO material, the sulfur content decreased to 0.16% which indicates, that during the nanohybrid synthesis, the sulfur was partially washed away. The presence of the porphyrin in the material was confirmed by the increased content of nitrogen in the hybrid. From the elemental analysis data, it was estimated that the prepared composite contains 3.3% of TPPH.

Table 1. The elemental analysis results of GO and TPPH-GO.

Sample	C wt.%	H wt.%	O* wt. %	N wt.%	S wt.%
GO	48.98	2.18	48.21	0.09	0.54
TPPH-GO	51.58	2.57	44.63	0.35	0.16

*oxygen content was calculated based on: 100% - residue after TGA [%] – C [%] – H [%] – S [%]

Optical absorption spectra

Absorption properties of TPPH

TPPH is only slightly soluble in water, thus all the experiments were performed in EtOH-H_2O (1:2 v/v) mixtures. The absorption spectrum of TPPH strongly depended on the pH. The UV-vis spectrum of TPPH at neutral pH exhibited a strong Soret band centered at ca. 418 nm (ε_{411}=4.2 × 10^5 M^{-1} cm^{-1}) and four less intense Q-bands at ca. 517, 555, 592 and 650 nm which are characteristic of the free base monomer (Figure 4). These spectra are consistent with reported results of earlier studies.[51] Spectrophotometric titration was employed to determine the acid dissociation constants over a wide pH range. Changes towards acidic or alkaline pH introduced

positive or negative charge, respectively, to neutral TPPH (Scheme 1). The change in spectra upon an addition of acid or base can be attributed to the attachment of two protons to the imino nitrogen atoms of the porphin ring or to the loss of the four protons from the hydroxyl group in the phenol substituents. Titration with hydrochloric acid led to a shift of the Soret band to 448 nm. In addition a new band arose at 322 nm, and the Q-band (650 nm) was broadened and red shifted to 688 nm. The three other Q bands disappeared under acidic conditions (Figure 4). The significant bathochromic shift of the Q band together with the increase in its intensity in acidic solution might be caused by charge transfer from the phenol groups to the porphyrin core.[52] Theoretical calculations also predicted that the HOMO-LUMO excitation in $TPPH^{2+}$ has charge transfer character (*vide infra*). It was found that the pK_a for the protonation of the imino nitrogens of the core is 4.8 (Figure S3), which is in agreement with previously reported data.[52] Thus, at pH<4.8 the TPPH exists as a diacidic monomer $TPPH^{2+}$. An increase in pH from neutral to alkaline pH caused the formation of the $THPP^{4-}$ anion due to deprotonation of the protons from the OH groups. In the UV-vis spectra at alkaline pH, the Soret band was broadened and red shifted toward 434 nm, and the two Q bands at 579 nm and 666 nm were present. The pK_a of the -OH groups in TPPH was determined to be 10.6 by a pH dependent UV-vis titration (Figure S3).

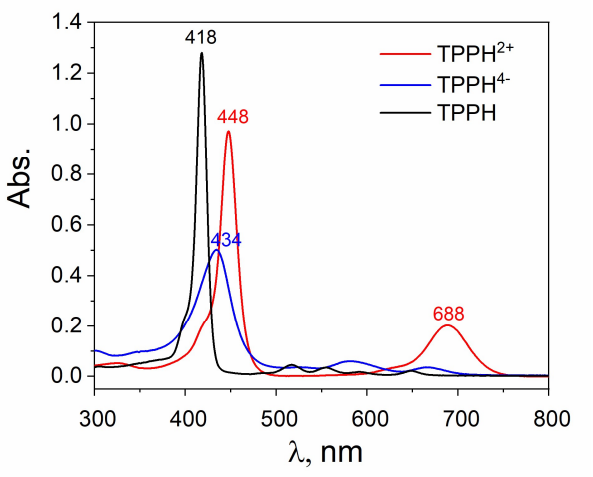

Figure 4. UV-Vis absorption spectra of 3.0 μM solution of TPPH- (pH 7.0) black line, $TPPH^{2+}$ - (pH 3.5) red line and $TPPH^{4-}$ - (pH 11.5) blue line.

Introduction of charge to the TPPH molecule upon changing the pH can influence the strength of its interaction with GO. Thus it was of interest to investigate the interaction of the three species: $TPPH^{2+}$, TPPH and $TPPH^{4-}$ with graphene oxide.

Absorption properties of TPPH in the presence of GO

The UV-vis spectroscopy was used to study the ground state interaction between both components: GO and neutral TPPH. UV-vis spectra are displayed in Figure 5A for a series of TPPH-GO nanohybrid suspensions (pH 6.8) measured for a constant TPPH concentration of 3.0 μM and for varying GO concentration. It is clear that GO had a remarkable effect on the UV-vis spectra. With increasing GO, the intensity of the porphyrin Soret band at 418 nm disappeared, and a new Soret band at 452 nm gradually increased. An isosbestic point was also observed at 428 nm. The location and number of Q bands changed. Three of the four Q bands completely disappeared, and a new broad band was observed at 699 nm. It can be noticed that the Soret band of the TPPH-GO exhibited a significant red-shift (34 nm). Our observations are different from the results reported by Zhu and co-workers.[16] In their study the Q bands did not disappear during the titration but were only shifted in comparison to free TPPH. However, these authors used reduced graphene oxide for which stronger π-π interactions with TPPH molecules are expected.

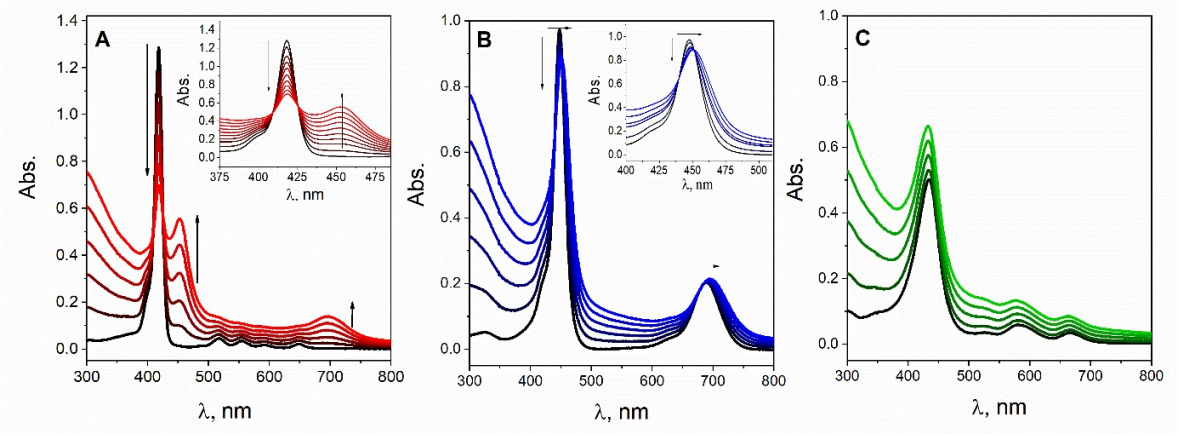

Figure 5. Absorption spectra measured during the process of titration of 3 ml of 3.0 μM EtOH-H_2O (1:2 v/v) solution of A) TPPH (pH 6.8), B) $TPPH^{2+}$ (pH 3.0), C) $TPPH^{4-}$ (pH 11.5) with 0.4 mg ml^{-1} of GO dispersion (0-0.025 mg ml^{-1}), the inset is the same spectra presented only in the Soret band region, spectra were not corrected for the GO absorption.

The significant similarity between the UV-vis spectra of TPPH-GO nanoassembly in Figure 5A to the UV-vis spectra of $TPPH^{2+}$ can be noticed. It may be explained by a partial charge transfer from the TPPH to the GO sheet, resulting in the formation of positive charge on the porphine core as in the $TPPH^{2+}$. This explanation is in agreement with our theoretical calculations (*vide infra*).

It was observed that the interaction of TPPH with GO was not as strong as for cationic porphyrins such as TMAP or TMPyP reported earlier.[18-20, 22] Even at high GO concentration 0.025 mg ml^{-1}, the Soret band attributed to free TPPH, unbound to GO, was present in the UV-vis spectra. To estimate what amount of the TPPH can be adsorbed on the GO surface, the absorption spectra of GO (0.1 mg ml^{-1}) were recorded with the addition of varying amounts of concentrated TPPH solution (Figure 6). With an increasing concentration of TPPH above 4.3 μM, we observed an increased contribution to the Soret band at 418 nm attributed to the free porphyrin. Based on this experiment, the maximum amount of TPPH adsorbed on the GO sheets was estimated to be ca.

0.03 mg per mg of GO. It was reported by Ge et.al that the percentage content of TPPH in the TPPH-GO composite was 3.6% [25] which is in good agreement with our work.

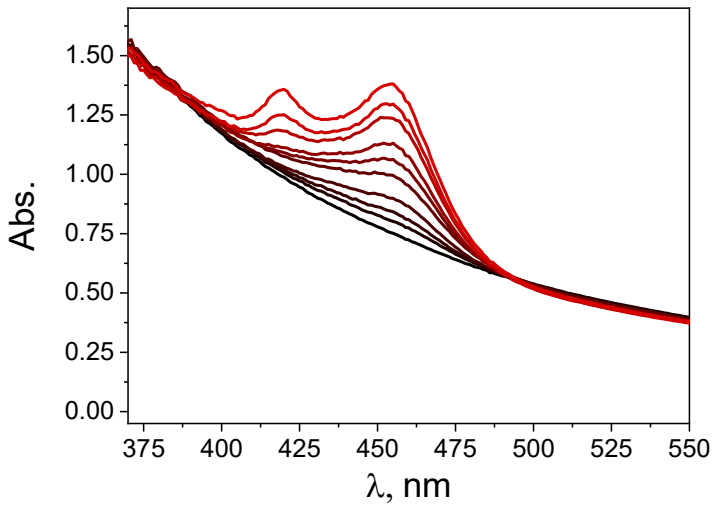

Figure 6. Absorption spectra recorded during addition of EtOH-H_2O (1:2 v/v) solution of TPPH (0-5.9 μM) to 0.1 mg ml^{-1} GO in H_2O (3 ml).

Interestingly, it was demonstrated earlier that the maximum amount of TPPH adsorbed on RGO sheets was ca. 0.11 mg per mg of RGO,[16] which is almost 4 times more than the maximum amount of TPPH that can be loaded onto the GO surface. Compared with GO, the large sp^2 conjugated network of reduced graphene oxide may facilitate strong π–π stacking interactions. Therefore, stronger π-π stacking interactions is feasible between TPPH and RGO.

These spectral results described above show that the interaction between TPPH and GO strongly influence the electronic structure of the porphyrin. The bathochromic shift (34 nm) of the Soret band observed upon nanohybrid formation could be explained by a flattening of the porphyrin molecule. Our hypothesis about TPPH flattening when adsorbed on the GO sheet is supported by the theoretical calculations on TPPH and TPPH-GO which predict that the dihedral angle between

the phenyl and porphyrin plane changes from 61° to 39.9° upon complexation with GO, which may be the reason for the batochromic shift of the Soret band.

π-π stacking and hydrogen bonding are the two types of interaction that could play a role in the formation of the stable nanohybrid composed of TPPH and GO components. The strength of hydrogen bonding was examined by replacing TPPH porphyrin by *meso*-tetra(4-methoxyphenyl)porphyrin (TPPOMe). The TPPOMe structure is analogous to the structure of TPPH but bears methoxy groups in the phenyl substituents instead of hydroxy groups. Due to lack of the solubility of the TPPOMe in EtOH-H_2O (1:2 v/v), the measurements were carried out in the mixture with higher EtOH content (EtOH-H_2O(5:1 v/v)). The UV-vis absorption spectra of TPPOMe with increasing amounts of GO are displayed in Figure 7. As can be seen, spectral changes upon titration of TPPOMe solution with the GO suspension were very similar to those observed during TPPH titration. Addition of GO resulted in a decrease of the Soret band intensity along with the development of a new red-shifted Soret band at 452 nm as well as a broad band at 692 nm.

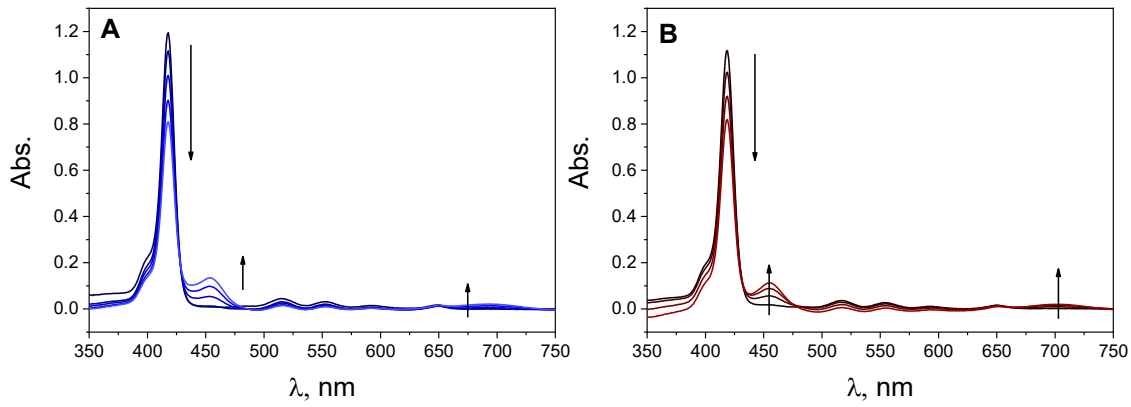

Figure 7. Absorption spectra recorded during the process of titration of 3 ml of 3.0 μM EtOH-H_2O (5:1 v/v) solution of A) TPPOMe, B) TPPH, with 2.0 mg ml^{-1} of GO dispersion (0-0.065 mg ml^{-1}), spectra were corrected for the GO absorption.

It is worth pointing out that significantly higher concentrations of GO were required to monitor the changes in the UV-vis of TPPOMe in comparison to TPPH. To determine whether this was the effect of a weaker interaction of TPPOMe with GO in comparison with TPPH or the effect of the solvent change, the TPPH titration with GO was repeated in an EtOH-H_2O mixture of (5:1 v/v). The observed spectral changes upon addition of GO to this TPPH solution were less pronounced than in the mixture with the higher water content. It can be concluded that the interaction between TPPH and GO in the mixture richer with ethanol was weaker, but still formation of the supramolecular assembly took place. For a higher GO concentration comparable with that used for TPPOMe experiment, the spectra changes were monitored. The Soret band shifted by 34 nm to 452 nm, and a new band at 688 nm arose. Based on these observations it can be stated that the strength of the interaction of the porphyrin TPPOMe with GO was similar to the strength of the interaction between TPPH and GO. This observation supports the hypothesis that π-π stacking interaction is required to form efficiently nanoassemblies with GO by simply mixing the solutions of both components. In the Ge et.al. work performed in EtOH even higher GO concentration (0.16 mg ml^{-1}) was necessary to observe UV-vis changes of TPPH upon GO addition.[25] This indicates that the solvent plays an important role in the efficiency of nanohybrid formation. Based on the experiments with the TPPOMe, it can be concluded that it is the π-π stacking that was responsible for the efficient assembly of TPPH onto the GO sheets.

Absorption properties of $TPPH^{2+}$ in the presence of GO

GO suspensions at neutral pH are negatively charged, thus it was expected that cationic porphyrin could be assembled onto their surfaces through electrostatic attraction and π-π stacking interactions. It was found that the pK_a of the carboxyl group in GO was 4.3, thus at low pH, the carboxyl groups of GO are mostly protonated.[53] On the other hand, the pK_a for the protonation of

the porphyrin core of TPPH was determined to be 4.8. In order to examine whether electrostatic attraction between $TPPH^{2+}$ and GO can favour formation of the nanohybrid, we performed measurements at pH 3. At this pH the electrostatic interaction was maximal since most of the porphyrin molecules exist as a dication and still GO has some percentage of deprotonated COOH groups. The absorption spectra of $TPPH^{2+}$ recorded with the addition of GO suspensions at pH 3 are shown in Figure 5B. A stronger interaction of $TPPH^{2+}$ with the GO compared to the TPPH was expected due to the introduction of positive charge on the porphyrin molecules. During titration of $TPPH^{2+}$ with graphene oxide, only small red shifts of the Soret band from 448 nm to 452 nm and long-wavelength band from 688 to 699 nm were observed (Figure 5B). Interestingly the formation of the $TPPH^{2+}$-GO nanohybrids resulted in only small changes in the UV-vis spectra as compared to TPPH-GO, which indicates that the electronic structure of $TPPH^{2+}$ is not affected as much as TPPH upon their adsorption onto GO sheets. It was postulated that charge transfer occurs during TPPH-GO formation which significantly effects the electronic structure of the porphyrin. This hypothesis is in agreement with the theoretical calculations. In the case of $TPPH^{2+}$ our theoretical calculations did not predict charge transfer for the HOMO-LUMO excitation. In addition the small red shift (4 nm) of the Soret band can be related to only a small change in the dihedral angle between the phenyl group and the porphine ring (from 39° to 33.7°) upon adsorption onto GO. Due to small spectral changes, the expected increase in the strength of the interaction between $TPPH^{2+}$ and GO based on the UV-vis titration experiment was not obvious. The lack of any meaningful spectroscopic changes of $TPPH^{2+}$ upon addition of GO does not exclude strong interaction between the moieties. It only indicates that the interaction with GO does not disturb strongly the electronic structure of the $TPPH^{2+}$.

The increase of the interaction strength between porphyrin and GO at pH 3 was confirmed by acidification of the TPPH and GO solution. Addition of the acid to the mixture of free neutral TPPH molecules not bounded to the GO and TPPH molecules adsorbed on the GO shifted the equilibrium toward the formation of the $TPPH^{2+}$-GO (Figure 8). Another argument in favor of efficient nanohybrid formation under acidic pH comes from a centrifuging experiment. The centrifugation process of the mixture of $TPPH^{2+}$ and GO allowed for an efficient nanohybrid isolation (Figure 1).

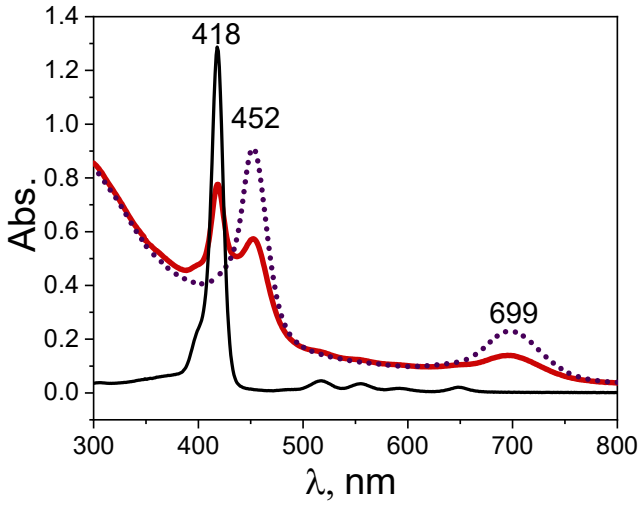

Figure 8. UV-Vis absorption spectra of 3.0 μM solution of TPPH (black line), mixture of TPPH with GO (0.025 mg ml^{-1}) (red line) and the same mixture after addition acid to pH 3 (dotted line).

The strength of the porphyrin interaction with GO at varying pH was evaluated using GO films. Solutions of 0.025 mg ml^{-1} GO (EtOH with 5% acetonitrile) were used for GO deposition onto glass slides covered with conducting fluorine-doped tin oxide (FTO). Deposition was performed electrochemically by applying a potential of 60 V for 2 minutes. During that process, partial reduction of the GO occurred. Subsequently, GO films were immersed into solutions containing TPPH (60 μM) at pH 6.8 or 3.0 for 2 h and rinsed with the solvent. After drying the films in air,

the absorption spectrum was measured. Obvious peaks around 464 nm and 726 nm that could be attributed to the absorption of the porphyrin were detected. It thereby confirms the porphyrin binding to GO film (Figure 9). These absorption bands were red-shifted with respect to the 452 nm and 699 nm absorption maxima of TPPH-GO in solution and might be related to the partial reduction of GO upon its deposition. It is clear that significantly more porphyrin molecules are adsorbed on GO film from the $TPPH^{2+}$ solution (pH 3.0). Based on the results discussed above, it can be stated that interaction of $TPPH^{2+}$ with GO sheets is stronger in acidic environment.

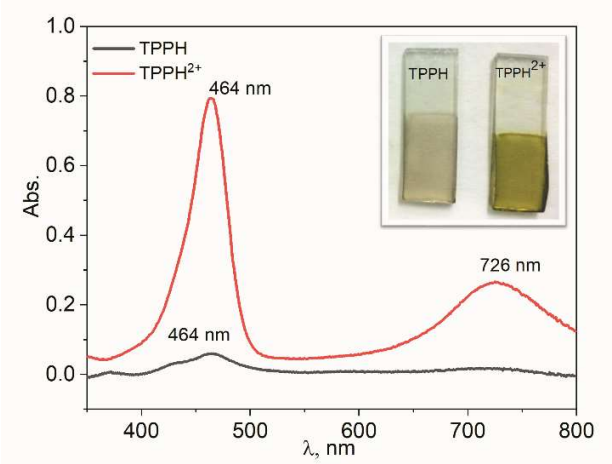

Figure 9. Adsorption of TPPH on GO films monitored by UV-vis spectroscopy. Absorption spectra of the FTO plate coated with GO immersed in solutions of TPPH (pH 6.8) (black line) and $TPPH^{2+}$ (pH 3.0) (red line), (spectra corrected for the absorption of GO film itself), inset: photographs of the films.

Absorption properties of $TPPH^{4-}$ in the presence of GO

The absorption spectra of $TPPH^{4-}$ recorded with the addition of GO suspension at pH 11.5 are shown in Figure 5C. During the measurements, the concentration of $TPPH^{4-}$ in water was kept constant at 3.0 μM, and the concentration of GO was varied from 0 to 0.02 mg ml^{-1} as the GO suspension was successively added into the dye solution. In the presence of GO no appreciable

changes in the UV-vis spectra of $TPPH^{4-}$ were registered, only an increase in the absorption that could be attributed to the absorption of GO was observed (Figure 5C). After the centrifuging of the suspension, practically all of the $TPPH^{4-}$ was left in the supernatant, and GO was collected as the precipitate (Figure S3). This indicates that the interaction between $TPPH^{4-}$ and GO is largely suppressed at basic pH. The weaker interaction of $TPPH^{4-}$ with GO can be explained by the electrostatic repulsion between negatively charged GO sheets and the porphyrin molecules.

Emission studies

Emission properties of TPPH and $TPPH^{2+}$ in the presence of GO

The interaction of the excited state of TPPH with the GO sheets was investigated by emission spectroscopy. One has to be aware that any quantitative analysis of fluorescence data of materials containing graphene is complicated due to, i.e., light absorption and scattering by the GO. Absorption of light by GO sheets can be taken into account by introducing the equation for the inner filter effect (Eq. S1).[54] In our study the correction factor for GO absorption of the excitation light amounted to as much as 24% for 0.018 mg ml^{-1} of GO. The necessity for the use of the inner filter correction is related to the relatively high concentration of GO required for efficient quenching of the emission. Another important issue is that when comparisons are made of emission data, it requires a matching of the absorbances at the excitation wavelength. In the current work, emission experiments for the TPPH-GO were performed with the excitation at the isosbestic point i.e. 428 nm, which ensured constant absorbance. TPPH itself has, in EtOH-H_2O (1:2 v/v), a broad emission comprising two unresolved Q(0,0) and Q(0,1) bands at ca. 657 and 719 nm, respectively, with a quantum yield of 0.13. (Figure 10A). This data are similar to those reported earlier for TPPH in chloroform.[51]

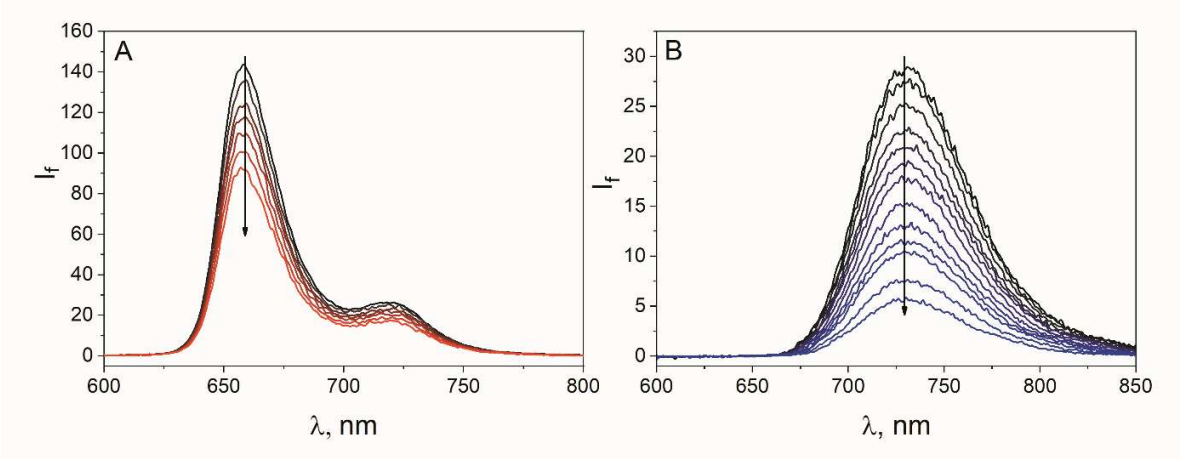

Figure 10. (A) Quenching of the fluorescence of 1.0 μM TPPH at pH 6.8 recorded during addition of an aqueous suspension of 0.4 mg ml^{-1} GO (0-0.009 mg ml^{-1}), λ_{exc} = 428 nm (B) Quenching of the fluorescence of 1.0 μM $TPPH^{2+}$ at pH 3.0 recorded during addition of an aqueous suspension of 0.4 mg ml^{-1} GO (0-0.009 mg ml^{-1}) λ_{exc} = 456 nm. Spectra corrected for inner filter effect.

A decrease in the TPPH fluorescence intensity is observed with increasing GO concentration.

Based on the emission measurements in the presence of graphene, one cannot specify unambiguously what is the quenching mechanisms although quenching of emission is often related to electron or energy transfer.[16, 33-34, 55] Since TPPH-GO has a different electronic structure as indicated by the change in its UV-vis absorption spectra compared to the absorption spectrum of unbound TPPH, any emission from the complex should be red shifted compared to that of free TPPH. Upon addition of GO suspension to the TPPH solution, no change in the shape as well as in the position of the peaks in the emission spectra were noticed. Moreover, as presented in Fig. 11, the fluorescence excitation spectrum recorded for the TPPH solution after addition of 0.02 mg ml^{-1} of GO, matched the absorption spectrum of free TPPH. The results discussed above, clearly demonstrates that TPPH-GO is not an emissive material and that the observed fluorescence in Figure 10A originates solely from the free TPPH (Scheme 3) in the suspension.

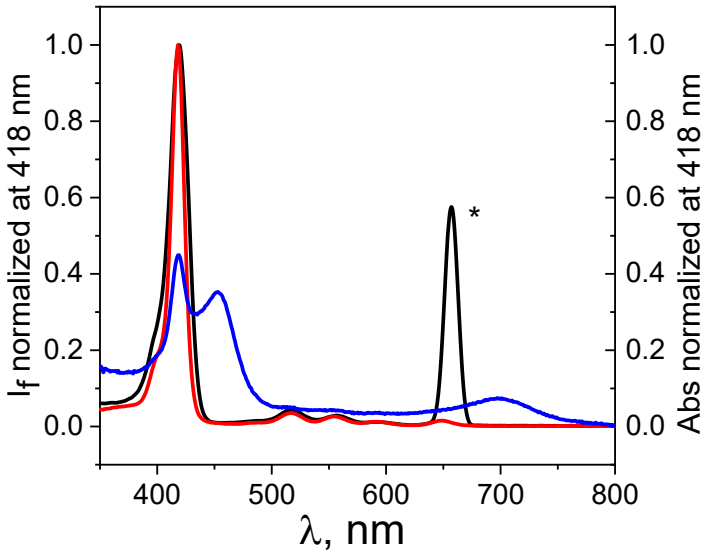

Figure 11. Normalized fluorescence excitation spectrum of the mixture of TPPH (0.8 μM) and GO (0.02 mg ml^{-1}) (black), absorption spectrum of this mixture (blue) and normalized absorption spectrum of TPPH (0.8 μM) in the absence of GO (red). Asterisk denotes scattered excitation light reaching to the detector.

The possible explanation for the lack of measurable emission from the TPPH-GO complex is the existence of a non-radiative process that leads to very quick deactivation of the singlet excited state. The recorded decrease of the fluorescence intensity upon addition of GO to the TPPH solution might also be attributed to dynamic quenching (Scheme 3) of an electronically excited state of free TPPH by GO. The question is whether this due to static or dynamic quenching.

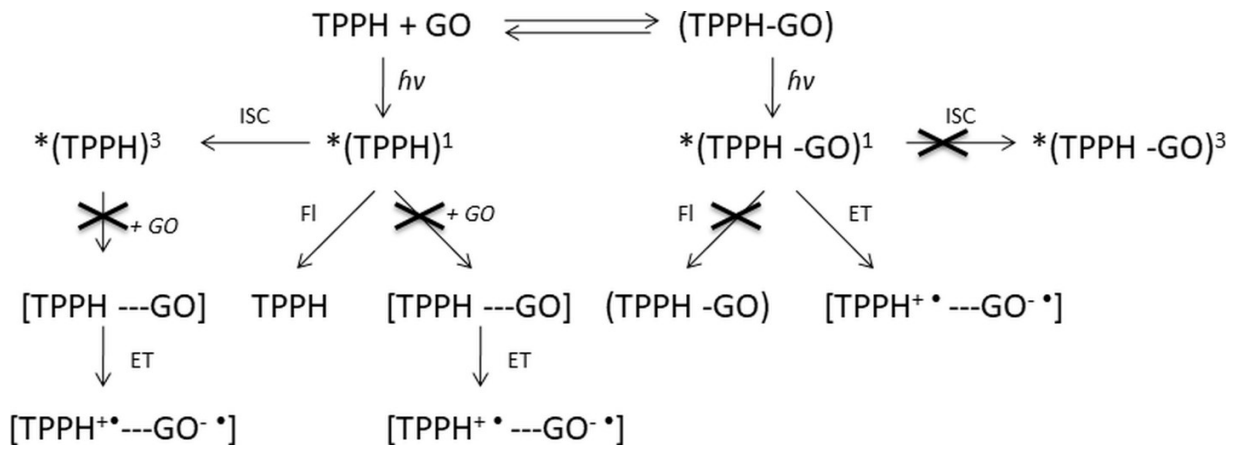

Scheme 3. Possible deactivation paths of the excited states of free TPPH and nanohybrid TPPH-GO discussed in text (Fl– fluorescence, ET - electron transfer).

This question was addressed by applying the time-correlated single photon counting technique. The emission decay profiles of TPPH were monitored in absence and presence of varying GO concentrations. The fluorescence lifetime calculated from the emission decay in the absence of GO was equal to 9.8 ns (excitation at 405 nm and monitoring at 657 nm). It was reported previously that the singlet excited state lifetime of TPPH in methanol was 12.2 ns. So the fluorescence lifetime of TPPH was shortened by ca. 2 ns in the presence of water.[56] After the addition of GO, no detectable change in the kinetic profiles of the excited state was recorded. One would normally have expected a shortening of the singlet excited state of unbound TPPH if the quenching were the result of a dynamic process induced by GO. There might also be the chance to see the appearance of a second decay associated with any fluorescence of the nanohybrid. Neither of these decays was detected during the time correlated single photon counting experiment. In Figure 12 there is displayed a comparison of the data obtained from the steady state and time resolved emission measurements.

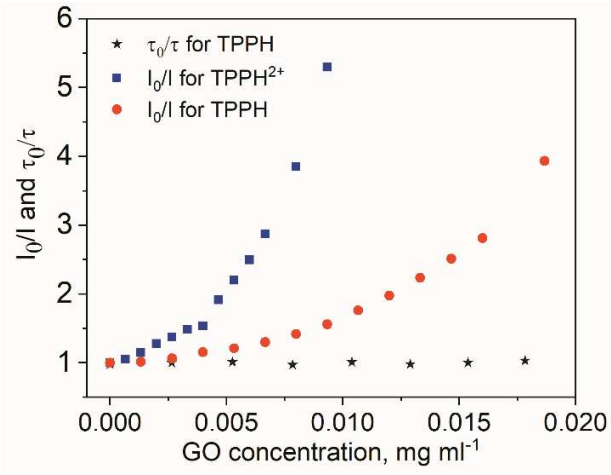

Figure 12. The relationship between fluorescence intensity I_0/I ($I_0 = I_f$ without GO, $I = I_f$ after addition of GO) and GO concentration for TPPH (red symbols) and $TPPH^{2+}$ (blue symbols) and the relationship between fluorescence lifetime τ_0/τ (τ_0 = fluorescence lifetime without GO, τ = fluorescence lifetime after addition of GO) and GO concentration for TPPH.

Based on the above time-resolved emission experiments, the possibility for dynamic quenching of the singlet excited state of free TPPH by GO can be eliminated (Scheme 3). In order to further confirm that the observed changes in the emission intensity upon addition of GO suspension to the TPPH solution can be solely attributed to the static quenching, the resolution of the absorption spectra into components was performed (details in SI). In short, a multi-linear regression analysis was applied to the absorption spectra recorded during the TPPH titration with GO in order to extract the individual concentrations of free TPPH and TPPH adsorbed on the GO surface for a series of different GO concentrations. Such a spectral resolution, that relies on Beer's Law, requires isolated reference spectra of all likely species, together with their molar absorption coefficients. The molar absorption coefficients for free TPPH were determined by measuring the UV-vis spectra of a solution of known concentration. The reference spectrum of the TPPH adsorbed on the GO was obtained based on the experiment described in Fig. 8 and making the

assumption that all TPPH molecules were adsorbed on GO. By using these two reference spectra, the experimental data were reproduced with reasonably good fit by applying a multi-linear regression method. A typical resolution is given in Figure 13A, and the resulting concentration profile for the change of free TPPH concentration upon addition of GO is displayed in Fig 13B. The change of the free TPPH concentration during the titration with the GO overlapped with the change of the emission intensity upon addition of GO to the solution of constant TPPH concentration (1.0 μM). These two sets of data are in very good agreement that undoubtedly proves that the observed decrease of the emission intensity can be solely related to static quenching.

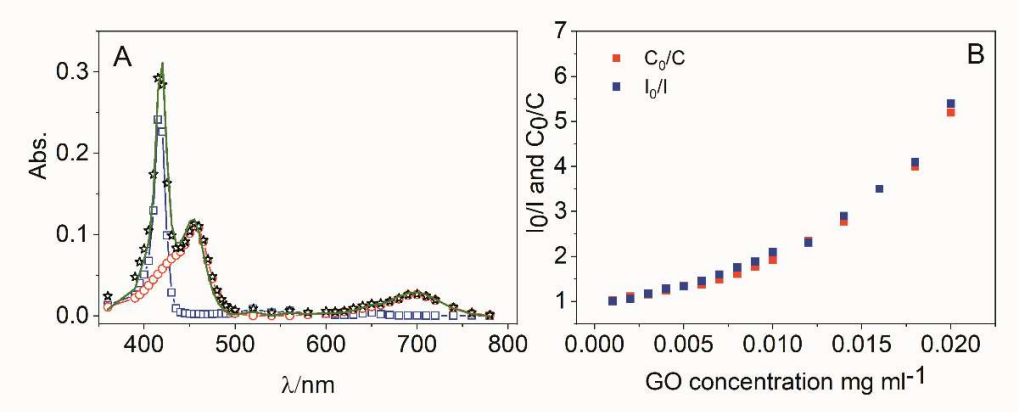

Figure 13. A) Exemplary resolution of UV-vis spectra for 1.0 μM EtOH-H_2O (1:2 v/v) solution of TPPH (pH 6.8) in the presence of 0.01 mg ml^{-1} of GO. The symbols represent □ for free TPPH, ○ for the TPPH adsorbed on GO, and * for the experimental data; solid green curve is the resulting fit from the regression analysis. B) The relationship between fluorescence intensity I_0/I and C_0/C ($I_0 = I_f$ without GO, $I = I_f$ after addition of GO, C_0 = initial concentration of free TPPH, C = concentration of free TPPH after addition of GO.

It is worth emphasizing here that, for the studied system, the decrease of the fluorescence intensity cannot be interpreted directly as evidence for an electron or an energy transfer process.

However, lack of detectable emission from the complex TPPH-GO points to the possibility of a very rapid deactivation process of the excited state such as electron or energy transfer.

Upon excitation at 456 nm (an isosbestic point for the titration with GO at acidic pH), $TPPH^{2+}$ (pH 3.0) exhibited a broad fluorescence band over the range of 680–820 nm, with a maximum at 730 nm in the absence of GO. As shown in Figure 10B we found that the successive addition of GO up to 0.009 mg ml^{-1} into the $TPPH^{2+}$ solution quenched the emission efficiently. As expected the decrease of the emission intensity is more pronounced for $TPPH^{2+}$ than for TPPH (Figure 12).

Femtosecond Transient Absorption Spectroscopy

To further elucidate the mechanism of the excited state interaction between TPPH and GO, femtosecond transient absorption spectroscopy was employed. Of special interest was an investigation of a possible electron transfer process occurring from the singlet excited state of the porphyrin to the graphene oxide sheets. The driving force of the electron transfer reaction was assessed using equation 1 [57]:

$$\Delta G_{ET} = E_{ox}(TPPH^{+}/TPPH) - E_{red}(GO/GO^{-}) - E_{0\text{-}0} \quad \text{(Eq 1)}$$

Where $E_{0\text{-}0}$ is the zero-zero transition of the singlet excited state of the TPPH, determined from the wavelength at the intersection of the normalized fluorescence and absorption spectra, $E_{0\text{-}0}$ = 1.89 eV. The oxidation potential of the TPPH was taken from the literature ($E_{ox}(TPPH^{+}/TPPH)$ = 0.81 V vs. NHE)[58]. It was reported that the degree of the oxidation of GO does not influence the conduction band edge and is always equal to -0.55 V vs. NHE.[59] Using the above mentioned values and Eq 1, the ΔG_{ET} for electron transfer from the TPPH singlet excited state to GO was calculated to be negative, ΔG_{ET}=–0.53 eV. The negative value for the free energy change of the electron transfer process suggests that a photoinduced electron transfer from TPPH to GO is feasible.

Femtosecond transient absorption experiments were performed at pH 3 in order to maximize the interaction between the porphyrin and GO and to minimize the contribution from the free porphyrin to the transient spectra. The singlet excited state difference absorption measured immediately after the 420 nm laser pulse excitation of $TPPH^{2+}$ at pH 3 showed a strong absorption around 475-600 nm and a Q-band bleach, whose position coincided with the Q band in the UV-vis absorption spectra of $TPPH^{2+}$ (ca. 448 and 688 nm). (See Figure 14A) The singlet excited state lifetime of $TPPH^{2+}$ obtained from the monoexponential fit to the decay profile at 500 nm was found to be 1.6 ns, which is in a good agreement with the same data obtained by the TCSPC technique. Interestingly, the decay of the signal from the singlet excited state over the whole time-window of the experiment (3 ns) was not accompanied by any distinct spectral evolution although small changes were noticeable. As the signal from the $^1(TPPH)^*$ was decreasing, there was simultaneous build-up of the low intensity signal around 650 nm, together with the isosbestic point at 615 nm. This 650 nm absorption can be identified as the absorption of the TPPH triplet excited state based on the similarity of the transient spectra obtained in the nanosecond flash photolysis experiment (Figure S4). Upon additions of GO to the $TPPH^{2+}$, the transient absorption showed very similar spectral features as the spectra registered for the free dye (See Figure 14B). The bleach has shifted to 700 nm as observed in the ground state UV-vis spectra.

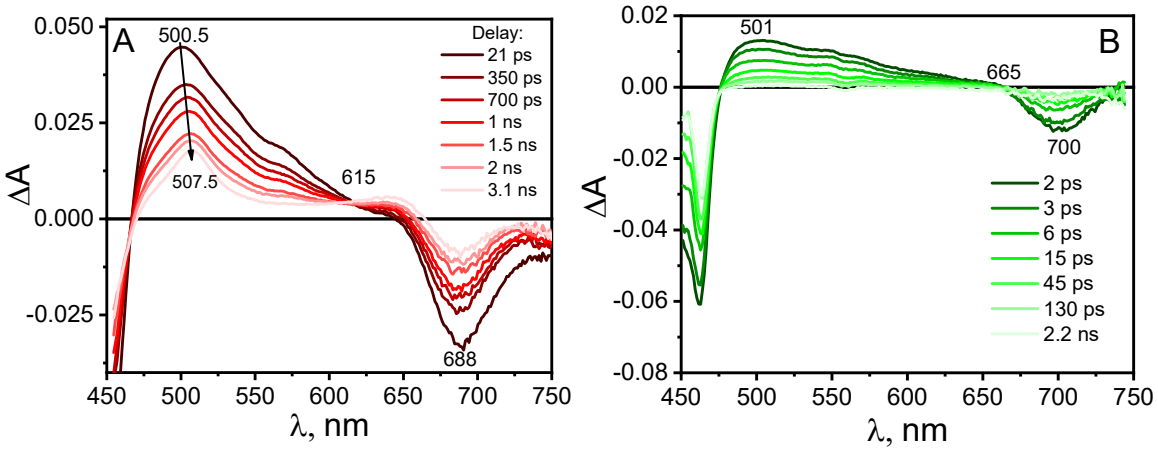

Figure 14. Transient absorption spectra registered at various time delays for (A) $TPPH^{2+}$ (3 μM) and (B) $TPPH^{2+}$-GO ([$TPPH^{2+}$] = 0.3 μM, [GO] = 0.1 mg ml^{-1}) in water (pH 3) following the 420 nm laser excitation.

Kinetic traces collected for $TPPH^{2+}$ in the absence and presence of GO for the same time window are given in Figure 15. While the kinetic profile at 501 nm of the singlet excited state of free $TPPH^{2+}$ did not decay over the first 100 ps, the analogous kinetic profile of the nanohybrid showed a very fast decay. Once $TPPH^{2+}$ is bound to the GO sheets, its singlet excited state lifetime was shortened to 12 ps that is evidence of an efficient interaction between the photoexcited dye molecules and the graphene oxide sheets. Even though no electron transfer products were detected (e.g. the radical cation of the porphyrin), it cannot be excluded that it is an electron transfer which in fact is responsible for the efficient quenching of the $TPPH^{2+}$ singlet excited state by the GO sheets. Such a conclusion can be rationalized by an efficient back electron transfer process, which would lead to the quenching of the excited state with no observable electron transfer products.

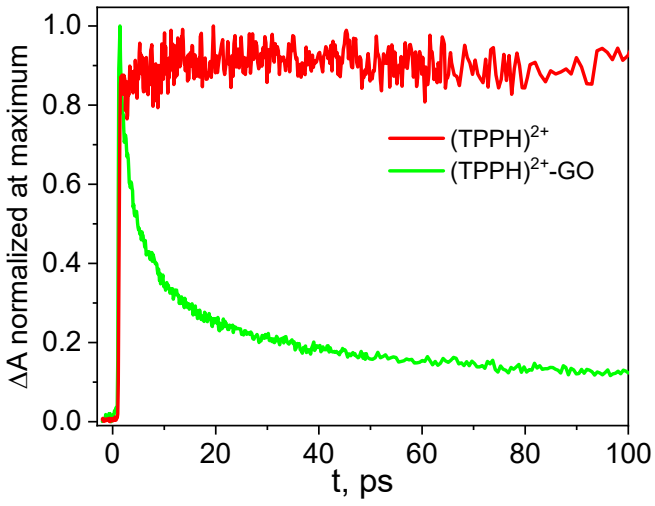

Figure 15. Transient absorption decays at 501 nm in water (pH 3) registered for the $TPPH^{2+}$ (red curve) and $TPPH^{2+}$-GO (green curve) following the 420 nm excitation.

Based on the similarity to other porphyrin-graphene type materials for which electron transfer processes were commonly found in femtosecond transient absorption experiments, it seems reasonable to attribute the fast decay of the singlet excited state of $TPPH^{2+}$ adsorbed on the GO to electron transfer processes.[20, 26] Furthermore Ge et. al. has shown that the introduction of the TPPH porphyrin largely enhanced the photocurrent of the GO.[25] Based on the minor spectral overlap between the emission of $TPPH^{2+}$ and the absorption of GO, energy transfer between the donor–acceptor components is highly unlikely. Taking all of these considerations into account, electron transfer seems to be the most plausible explanation for the significant shortening of the singlet excited state of $TPPH^{2+}$.

The residual absorbance of about 10% appeared in all the recorded traces, and it is attributed to the absorption of the singlet excited state of free $TPPH^{2+}$ that was not absorbed onto the GO surface.

Nanosecond flash photolysis

Nanosecond transient absorption experiments were performed to probe whether the triplet state of $TPPH^{2+}$ could be quenched by GO. Upon laser excitation at 355 nm, $TPPH^{2+}$ exhibited a strong bleaching of the ground state at 450 nm and 690 nm, and the triplet state absorption with two bands with maxima at 510 nm and 645 nm (Figure S4). The triplet lifetime of 100 μs was obtained from a monoexponential fit of the bleach recovery at 440 nm. This value is similar to the reported triplet lifetime of TPPH in methanol (120 μs).[30] The intensity of the transient absorption spectra decreased significantly upon addition of GO, and, at high GO content, the triplet state of $TPPH^{2+}$ is not populated at all. From this observation, it can be concluded that intersystem crossing in $TPPH^{2+}$ cannot compete with the very fast process deactivating the singlet excited state when $TPPH^{2+}$ is complexed to GO. Figure 16 shows kinetic profiles at 440 nm registered for $TPPH^{2+}$ in

the absence and presence of GO upon laser excitation at 355 nm. (The added amount of GO was low enough such that free $TPPH^{2+}$ was still present in the solution.) No change in the bleach recovery was observed upon addition of GO (Figure 16). On the basis of this result it can be stated that triplet state of the $TPPH^{2+}$ is not quenched by GO, no dynamic quenching.

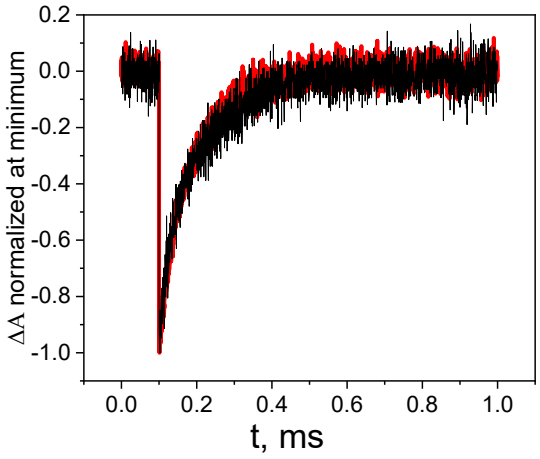

Figure 16. Normalized profiles of bleach recovery monitored at 440 nm obtained during laser flash photolysis (with excitation at 355 nm) of deoxygenated solutions of $TPPH^{2+}$(5 μM) (red) and for $TPPH^{2+}$ in the presence of GO (0.005 mg ml^{-1}) (black).

Theoretical calculations

DFT calculations at the BP86+D3gCP/def2-TZVP level were performed to predict the structures of the ground states of TPPH and $TPPH^{2+}$. The optimized ground state geometries of these two forms of porphyrin are provided at the top of Figure 17, together with selected bond angles and dihedral angles.

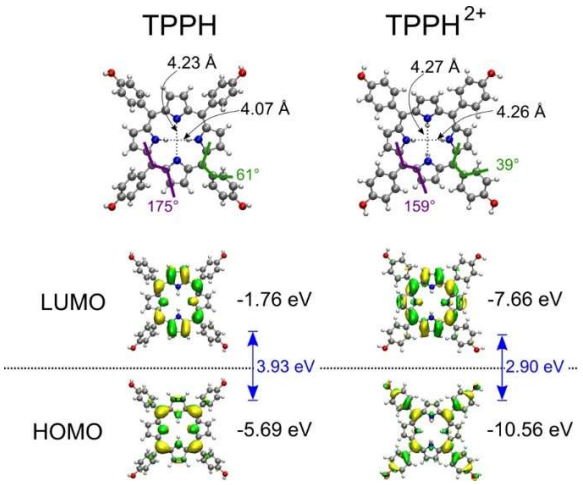

Figure 17. Top: calculated (BP86+D3gCP/def2-TZVP) structures of TPPH and $TPPH^{2+}$. Bottom: ±0.03 a.u. isosurface plots of HOMO and LUMO along with corresponding orbital energies obtained at the BHLYP/def2-TZVP level.

Results of the calculations show that while TPPH brings about a slight out-of-plane distortion from the planar structure of the macrocycle within 5°, the protonation of the porphyrin core gives rise to a distortion from planarity of 20°. It can be attributed to repulsive interactions between the H atoms bonded to core N atoms.[60] In the structure of the TPPH molecule there are four phenol rings, which are attached to the carbon atoms of the porphyrin core. The phenol fragments are not located in the plane of the porphyrin core due to steric hindrance. With reference to the average plane of the macrocycle, the phenol substituents are tilted by an angle of about 61° for the nonprotonated structures, and only about 39° for protonated $TPPH^{2+}$. Thus, the protonation of the porphyrin core, in addition to causing deviation from planarity of the macrocycle, also simply decreases the tilt angles of the phenyl substituent groups. This is in agreement with previous literature findings on *meso*-substituents porphyrin.[60]

The isosurface plots of the highest occupied and lowest unoccupied molecular orbitals (HOMO and LUMO, respectively) for TPPH and $TPPH^{2+}$ are depicted at the bottom of Figure 17. The

results of the calculations indicate that for $TPPH^{2+}$ the HOMO has significant contribution at the phenyl rings due to small tilt angles of the phenyl substituents relative to the porphyrin core that allows for efficient hybridization of the phenyl π orbitals with the porphyrin delocalized orbitals. Thus, the charge transfer character of the HOMO-LUMO transition in $TPPH^{2+}$ will be more pronounced as compared to TPPH and can be responsible for the appearance of the red-shifted band at 688 nm in the ground state UV-vis absorption spectra.

Next we determined the geometric and electronic structures of the complexes of GO with TPPH and $TPPH^{2+}$ (see Figure 18). The main focus was in an elucidation of the difference in the interaction between TPPH and $TPPH^{2+}$ with GO. The geometry of the TPPH molecule in the complex with graphene differs significantly from the geometry of the isolated TPPH molecule. The main difference can be seen in the reduction of the twisting angles of the phenol rings relative to the plane of the porphine core and in the nonplanar configuration of the porphyrin core of the TPPH molecule in the complex with graphene oxide. The interaction of TPPH with graphene oxide leads to a twisting of the side rings relative to the porphyrin core from 61° to 40°. On the other hand, the interaction of protonated $TPPH^{2+}$ with graphene leads to a negligible decrease of the dihedral angle between the plane of the porphyrin and side ring from 39° to 34°. This is in agreement with the observed small shift of the Soret band upon the addition of GO. As presented in Figure 18 the HOMO, for both of the investigated complexes, is located on the porphyrin entity. Also, the LUMO for $TPPH^{2+}$-GO is located primarily on the porphyrin entity whereas, for the TPPH-GO, the LUMO orbital is located on the GO. Thus, the decrease of the dihedral angle by 21° along with the charge transfer character of the HOMO-LUMO transition for the TPPH-GO complex explains the observed significant changes in its UV-vis spectra i.e. the red shift of the Soret band by 34 nm and the built up of the new band with a maximum at 699 nm.

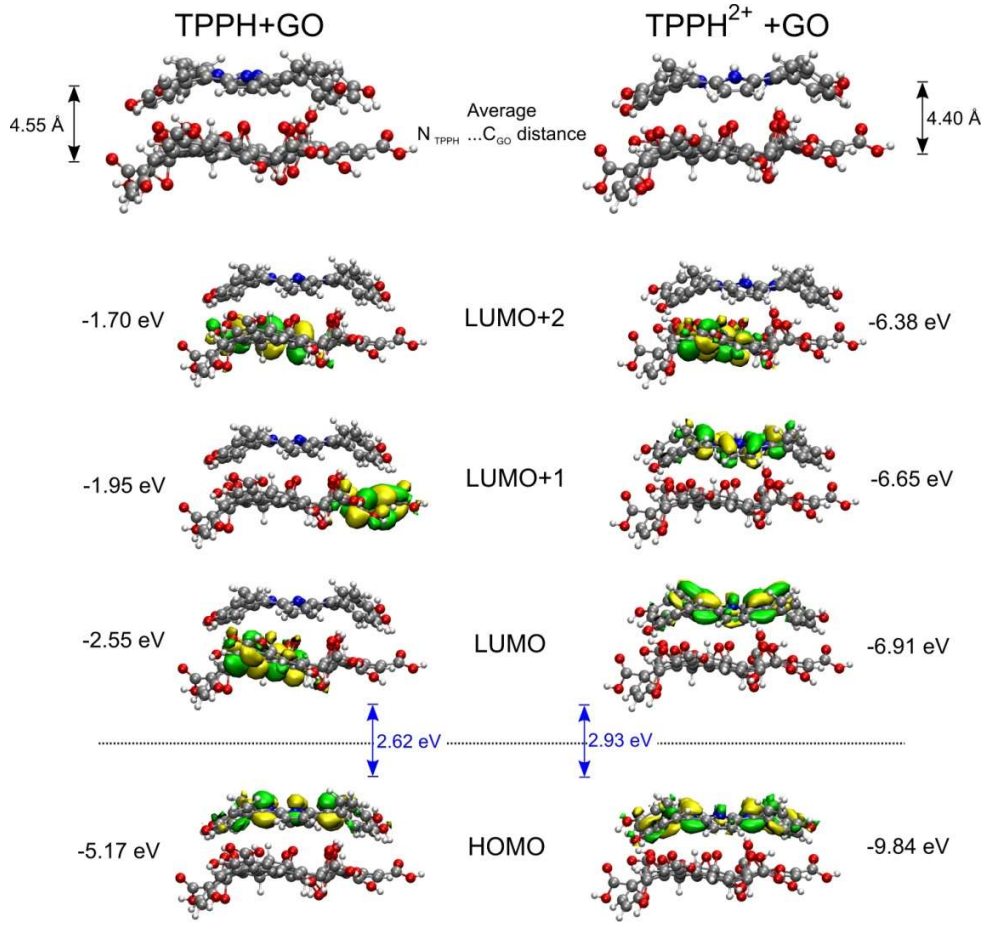

Figure 18. Top: Calculated (BP86+D3gCP/def2-TZVP) structures of TPPH-GO and $TPPH^{2+}$-GO complexes. Bottom: ±0.03 a.u. isosurface plots of selected frontier orbitals along with corresponding orbital energies obtained at the BHLYP/def2-TZVP level.

In order to compare the strengths of the interaction of TPPH and $TPPH^{2+}$ with GO, the interaction energies were calculated. The values of these energies are -22.4 kcal mol^{-1} and -58.0 kcal mol^{-1} for TPPH-GO and $TPPH^{2+}$-GO, respectively. In agreement with our experimental findings, the theoretical calculations also predict a stronger interaction between $TPPH^{2+}$ and GO than for TPPH and GO. In addition the center-to-center distance between $TPPH^{2+}$ and GO was found to be 4.4 Å in comparison to 4.55 Å found for the TPPH-GO nanohybrid. Therefore, the

effective interaction and electronic coupling matrix element between graphene oxide and porphyrin will be stronger in the former case.

Conclusions

In conclusion, two points should be emphasized. First, fundamental insight is that quantiative emission measurements for graphene based materials should take into account the inner filter correction for the GO absorption as well as a careful choice of the excitation wavelength in order to keep constant absorbance. One has to be aware that quantitative analysis of the data derived from absorption and emission data obtained for graphene based materials needs to be done with caution.

Secondly, both TPPH and $TPPH^{2+}$ molecules can be assembled onto the surface of the graphene oxide, but it was clearly shown that the stronger interaction with GO occurred for $TPPH^{2+}$. It was demonstrated, by efficient isolation of the $TPPH^{2+}$-GO complex and film formation, that $TPPH^{2+}$ adsorbed on the GO surface more efficiently than did neutral TPPH. Experimental results are in full agreement with the theoretical calculations. Stronger interaction in acidic environment can be rationalized by the electrostatic attraction between positively charged $TPPH^{2+}$ and negatively charged GO. Such interactions are not present for neutral TPPH. Our comprehensive analysis of the emission quenching led to the conclusion that it is solely attributed to static quenching of the porphyrin. Surprisingly, fluorescence was not detected for the nanohybrid which indicates that a very fast deactivation process must take place. Ultrafast time-resolved transient absorption spectroscopy demonstrates that although the singlet excited state lifetime of $TPPH^{2+}$ was decreased in the presence of the GO from 1.4 ns to 12 ps, no electron transfer products were detected. It is highly plausible that shortening of the singlet excited state lifetime of $TPPH^{2+}$ can be attributed to

the electron transfer and that the lack of the electron transfer products is related to fast back electron transfer.

ASSOCIATED CONTENT

Supporting Information

Absorption spectra of TPPH and $TPPH^{4-}$ with the addition of GO suspension and spectrum of the supernatant after centrifuging, UV-Vis spectra of acid-base titration of TPPH, equation for inner filter effect and details information on UV-vis spectra resolution, transient absorption spectra obtained from nanosecond flash photolysis, Cartesian coordinates for TPPH, $TPPH^{2+}$, GO and nanohybrids.

AUTHOR INFORMATION

Corresponding Author

***Email: alewand@amu.edu.pl**

Funding Sources

This research was financially supported by the National Science Centre (project no. 2015/19/D/ST5/00682). A. K. was partially supported by the Ministry for Science and Higher Education, Poland via fellowship no. 093/STYP/11/2016.

Conflicts of interest

There are no conflicts to declare

ACKNOWLEDGMENT

This research was financially supported by the National Science Centre (project no. 2015/19/D/ST5/00682). This is document number NDRL 5227 from the Notre Dame Radiation Laboratory. The authors are thankful to Dr. T. Pedzinski for his help in femtosecond transient

absorption spectroscopy measurements. E. G. thanks the Director of the Notre Dame Radiation Laboratory for a stipend that supported part of this work. A. K. acknowledges Ministry for Science and Higher Education, Poland for partial support via fellowship no. 093/STYP/11/2016. Access to high performance computing resources was provided by the Interdisciplinary Centre for Mathematical and Computational Modelling in Warsaw, Poland, under grant no. G64-9.

References:

1. Kamat, P. V., Graphene-Based Nanoarchitectures. Anchoring Semiconductor and Metal Nanoparticles on a Two-Dimensional Carbon Support. *J. Phys. Chem. Lett.* **2010**, *1*, 520-527.

2. Rao, C. N. R.; Sood, A. K.; Subrahmanyam, K. S.; Govindaraj, A., Graphene: The New Two-Dimensional Nanomaterial. *Angew. Chem. Int. Ed.* **2009**, *48*, 7752-7777.

3. Rao, C. N. R.; Sood, A. K.; Voggu, R.; Subrahmanyam, K. S., Some Novel Attributes of Graphene. *J. Phys. Chem. Lett.* **2010**, *1*, 572-580.

4. Novoselov, K. S.; Geim, A. K.; Morozov, S. V.; Jiang, D.; Katsnelson, M. I.; Grigorieva, I. V.; Dubonos, S. V.; Firsov, A. A., Two-Dimensional Gas of Massless Dirac Fermions in Graphene. *Nature* **2005**, *438*, 197-200.

5. Geim, A. K.; Novoselov, K. S., The Rise of Graphene. *Nat. Mater.* **2007**, *6*, 183-191.

6. Kiessling, D., et al., Novel Nanographene/Porphyrin Hybrids - Preparation, Characterization, and Application in Solar Energy Conversion Schemes. *Chem. Sci.* **2013**, *4*, 3085-3098.

7. Guancai, X.; Kai, Z.; Beidou, G.; Qian, L.; Liang, F.; Ru, G. J., Graphene-Based Materials for Hydrogen Generation from Light-Driven Water Splitting. *Adv. Mater.* **2013**, *25*, 3820-3839.

8. Georgakilas, V.; Otyepka, M.; Bourlinos, A. B.; Chandra, V.; Kim, N.; Kemp, K. C.; Hobza, P.; Zboril, R.; Kim, K. S., Functionalization of Graphene: Covalent and Non-Covalent Approaches, Derivatives and Applications. *Chem. Rev.* **2012**, *112*, 6156-6214.

9. Chen, D.; Feng, H.; Li, J., Graphene Oxide: Preparation, Functionalization, and Electrochemical Applications. *Chem. Rev.* **2012**, *112*, 6027-6053.

10. Lightcap, I. V.; Kamat, P. V., Graphitic Design: Prospects of Graphene-Based Nanocomposites for Solar Energy Conversion, Storage, and Sensing. *Acc. Chem. Res.* **2013**, *46*, 2235-2243.

11. Kamat, P. V., Graphene-Based Nanoassemblies for Energy Conversion. *J. Phys. Chem. Lett.* **2011**, *2*, 242-251.

12. G. Shao, Y. L., F. Wu, C. Yang, F. Zeng and Q. Wu, Graphene Oxide: The Mechanisms of Oxidation and Exfoliation. *J. Mat. Sci* **2012**, *47*, 4400-4409.

13. Dave, S. H.; Gong, C.; Robertson, A. W.; Warner, J. H.; Grossman, J. C., Chemistry and Structure of Graphene Oxide Via Direct Imaging. *ACS Nano* **2016**, *10*, 7515-7522.

14. Dreyer, D. R.; Park, S.; Bielawski, C. W.; Ruoff, R. S., The Chemistry of Graphene Oxide. *Chem. Soc. Rev.* **2010**, *39*, 228-240.

15. Ladomenou, K.; Natali, M.; Iengo, E.; Charalampidis, G.; Scandola, F.; Coutsolelos, A. G., Photochemical Hydrogen Generation with Porphyrin-Based Systems. *Coord. Chem. Rev.* **2015**, *304-305*, 38-54.

16. Zhu, M.; Li, Z.; Xiao, B.; Lu, Y.; Du, Y.; Yang, P.; Wang, X., Surfactant Assistance in Improvement of Photocatalytic Hydrogen Production with the Porphyrin Noncovalently Functionalized Graphene Nanocomposite. *ACS Appl. Mater. Interfaces* **2013**, *5*, 1732-1740.

17. Yuan, Y.-J.; Chen, D.; Zhong, J.; Yang, L.-X.; Wang, J.-J.; Yu, Z.-T.; Zou, Z.-G., Construction of a Noble-Metal-Free Photocatalytic H2 Evolution System Using Mos2/Reduced Graphene Oxide Catalyst and Zinc Porphyrin Photosensitizer. *J. Phys. Chem. C* **2017**, *121*, 24452-24462.

18. Ye, T.-x.; Ye, S.-l.; Chen, D.-m.; Chen, Q.-a.; Qiu, B.; Chen, X., Spectroscopic Characterization of Tetracationic Porphyrins and Their Noncovalent Functionalization with Graphene. *Spectrochim. Acta A* **2012**, *86*, 467-471.

19. Xu, Y.; Zhao, L.; Bai, H.; Hong, W.; Li, C.; Shi, G., Chemically Converted Graphene Induced Molecular Flattening of 5,10,15,20-Tetrakis(1-Methyl-4-Pyridinio)Porphyrin and Its Application for Optical Detection of Cadmium(Ii) Ions. *J. Am. Chem. Soc.* **2009**, *131*, 13490-13497.

20. Wojcik, A.; Kamat, P. V., Reduced Graphene Oxide and Porphyrin. An Interactive Affair in 2-D. *ACS Nano* **2010**, *4*, 6697-6706.

21. Wang, Y.; Zhang, Y.; Chen, J.; Dong, Z.; Chang, X.; Zhang, Y., A Photoinduced Electron Transfer System by Graphene Oxide Non-Covalently Linked Porphyrin Antennae in Water. *Electrochemistry* **2015**, *83*, 950-955.

22. Masih, D.; Aly, S. M.; Usman, A.; Alarousu, E.; Mohammed, O. F., Real-Time Observation of Ultrafast Electron Injection at Graphene-Zn Porphyrin Interfaces. *Phys. Chem. Chem. Phys.* **2015**, *17*, 9015-9019.

23. Liu, Z. D.; Zhao, H. X.; Huang, C. Z., Obstruction of Photoinduced Electron Transfer from Excited Porphyrin to Graphene Oxide: A Fluorescence Turn-on Sensing Platform for Iron (Iii) Ions. *PLoS ONE 7* **2012**, *7*, e 50367.

24. Geng, J.; Jung, H.-T., Porphyrin Functionalized Graphene Sheets in Aqueous Suspensions: From the Preparation of Graphene Sheets to Highly Conductive Graphene Films. *J. Phys. Chem. C* **2010**, *114*, 8227-8234.

25. Ge, R.; Wang, X.; Zhang, C.; Kang, S.-Z.; Qin, L.; Li, G.; Li, X., The Influence of Combination Mode on the Structure and Properties of Porphyrin–Graphene Oxide Composites. *Colloids Surf. A* **2015**, *483*, 45-52.

26. Aly, S. M.; Parida, M. R.; Alarousu, E.; Mohammed, O. F., Ultrafast Electron Injection at the Cationic Porphyrin-Graphene Interface Assisted by Molecular Flattening. *Chem. Commun.* **2014**, *50*, 10452-10455.

27. Guo, P.; Chen, P.; Liu, M., One-Dimensional Porphyrin Nanoassemblies Assisted Via Graphene Oxide: Sheetlike Functional Surfactant and Enhanced Photocatalytic Behaviors. *ACS Appl. Mater. Interfaces* **2013**, *5*, 5336-5345.

28. Bonnett, R.; White, R. D.; Winfield, U. J.; Berenbaum, M. C., Hydroporphyrins of the Meso-Tetra(Hydroxyphenyl)Porphyrin Series as Tumour Photosensitizers. *Biochemical Journal* **1989**, *261*, 277-280.

29. Chen, Y.; Huang, Z.-H.; Yue, M.; Kang, F., Integrating Porphyrin Nanoparticles into a 2d Graphene Matrix for Free-Standing Nanohybrid Films with Enhanced Visible-Light Photocatalytic Activity. *Nanoscale* **2014**, *6*, 978-985.

30. Bonnett, R.; Charlesworth, P.; D. Djelal, B.; Foley, S.; J. McGarvey, D.; George Truscott, T., Photophysical Properties of 5,10,15,20-Tetrakis(M-Hydroxyphenyl)Porphyrin (M-Thpp), 5,10,15,20-Tetrakis(M-Hydroxyphenyl)Chlorin (M-Thpc) and 5,10,15,20-Tetrakis(M-Hydroxyphenyl)Bacteriochlorin (M-Thpbc): A Comparative Study. *Journal of the Chemical Society, Perkin Transactions 2* **1999**, 325-328.

31. Wang, Y. T.; Chang, X. Y.; Zhang, Y.; Zhang, J. Q., Non-Covalent Porphyrin-Graphene Oxide Donor-Acceptor Photoinduced Electron Transfer Nanohybrids as Ph Regulated Light-Harvesting Model. *J. Nanosci. Nanotechnol.* **2017**, *17*, 9027-9035.

32. Min, S.; Lu, G., Dye-Sensitized Reduced Graphene Oxide Photocatalysts for Highly Efficient Visible-Light-Driven Water Reduction. *J. Phys. Chem. C* **2011**, *115*, 13938-13945.

33. Min, S.; Lu, G., Dye-Cosensitized Graphene/Pt Photocatalyst for High Efficient Visible Light Hydrogen Evolution. *Int. J. Hydrog. Energy* **2012**, *37*, 10564-10574.

34. Mou, Z.; Dong, Y.; Li, S.; Du, Y.; Wang, X.; Yang, P.; Wang, S., Eosin Y Functionalized Graphene for Photocatalytic Hydrogen Production from Water. *Int. J. Hydrog. Energy* **2011**, *36*, 8885-8893.

35. Stobinski, L.; Lesiak, B.; Malolepszy, A.; Mazurkiewicz, M.; Mierzwa, B.; Zemek, J.; Jiricek, P.; Bieloshapka, I., Graphene Oxide and Reduced Graphene Oxide Studied by the Xrd, Tem and Electron Spectroscopy Methods. *J. Electron. Spectrosc. Relat. Phenom.* **2014**, *195*, 145-154.

36. Pedzinski, T., Markiewicz, A. Marciniak, B. , Photosensitized Oxidation of Methionine Derivatives. Laser Flash Photolysis Studies. *Res. Chem. Intermed.* **2009**, *35*, 497-506.

37. Neese, F., The Orca Program System. *Wiley Interdiscip. Rev. Comput. Mol. Sci* **2012**, *2*, 73-78.

38. Neese, F., Software Update: The Orca Program System, Version 4.0. . *Wiley Interdiscip. Rev. Comput. Mol. Sci* **2018**, *8*, e1327.

39. Becke, A. D., Density-Functional Exchange-Energy Approximation with Correct Asymptotic Behavior. *Phys. Rev. A* **1988**, *38*, 3098-3100.

40. Perdew, J. P., Density-Functional Approximation for the Correlation Energy of the Inhomogeneous Electron Gas. *Phys. Rev. B* **1986**, *33*, 8822-8824.

41. Becke, A. D., A New Mixing of Hartree–Fock and Local Density-Functional Theories. *J. Chem. Phys.* **1993**, *98*, 1372-1377.

42. Dreuw, A.; Weisman, J. L.; Head-Gordon, M., Long-Range Charge-Transfer Excited States in Time-Dependent Density Functional Theory Require Non-Local Exchange. *J. Chem. Phys.* **2003**, *119*, 2943-2946.

43. Weigend, F.; Ahlrichs, R., Balanced Basis Sets of Split Valence, Triple Zeta Valence and Quadruple Zeta Valence Quality for H to Rn: Design and Assessment of Accuracy. *Phys. Chem. Chem. Phys.* **2005**, *7*, 3297-3305.

44. Grimme, S.; Antony, J.; Ehrlich, S.; Krieg, H., A Consistent and Accurate Ab Initio Parametrization of Density Functional Dispersion Correction (Dft-D) for the 94 Elements H-Pu. *J. Chem. Phys.* **2010**, *132*, 154104.

45. Grimme, S.; Ehrlich, S.; Goerigk, L., Effect of the Damping Function in Dispersion Corrected Density Functional Theory. *J. Comput. Chem.* **2011**, *32*, 1456-1465.

46. Kruse, H.; Grimme, S., A Geometrical Correction for the Inter- and Intra-Molecular Basis Set Superposition Error in Hartree-Fock and Density Functional Theory Calculations for Large Systems. *J. Chem. Phys.* **2012**, *136*, 154101.

47. Weigend, F., Accurate Coulomb-Fitting Basis Sets for H to Rn. *Phys. Chem. Chem. Phys.* **2006**, *8*, 1057-1065.

48. Izsák, R.; Neese, F., An Overlap Fitted Chain of Spheres Exchange Method. *J. Chem. Phys.* **2011**, *135*, 144105.

49. He, H.; Klinowski, J.; Forster, M.; Lerf, A., A New Structural Model for Graphite Oxide. *Chem. Phys. Lett.* **1998**, *287*, 53-56.

50. Dimiev, A. M.; Tour, J. M., Mechanism of Graphene Oxide Formation. *ACS Nano* **2014**, *8*, 3060-3068.

51. Rojkiewicz, M.; Kuś, P.; Kozub, P.; Kempa, M., The Synthesis of New Potential Photosensitizers [1]. Part 2. Tetrakis-(Hydroxyphenyl)Porphyrins with Long Alkyl Chain in the Molecule. *Dyes Pigm.* **2013**, *99*, 627-635.

52. J, S.; Tønnesen, H. H.; Kristensen, S., Influence of Aqueous Media Properties on Aggregation and Solubility of Four Structurally Related Meso-Porphyrin Photosensitizers Evaluated by Spectrophotometric Measurements. *Die Pharmazie - An International Journal of Pharmaceutical Sciences* **2013**, *68*, 100-109.

53. Orth, E. S.; Ferreira, J. G. L.; Fonsaca, J. E. S.; Blaskievicz, S. F.; Domingues, S. H.; Dasgupta, A.; Terrones, M.; Zarbin, A. J. G., Pka Determination of Graphene-Like Materials: Validating Chemical Functionalization. *J. Colloid Interface Sci.* **2016**, *467*, 239-244.

54. Marciniak, B., Does Cu(Acac)2 Quench Benzene Fluorescence?: A Physical Chemistry Experiment. *J. Chem. Educ.* **1986**, *63*, 998-1000.

55. Zhang, W.; Li, Y.; Peng, S., Facile Synthesis of Graphene Sponge from Graphene Oxide for Efficient Dye-Sensitized H2 Evolution. *ACS Appl. Mater. Interfaces* **2016**, *8*, 15187-15195.

56. Bonnett, R.; McGarvey, D. J.; Harriman, A.; Land, E. J.; Truscott, T. G.; Winfield, U.-J., Photophysical Properties of Meso-Tetraphenylporphyrin and Some Meso-Tetra(Hydroxyphenyl)Porphyrins. *Photochem. Photobiol.* **1988**, *48*, 271-276.

57. Weller, A., Photoinduced Electron Transfer in Solution: Exciplex and Radical Ion Pair Formation Free Enthalpies and Their Solvent Dependence. *Zeitschrift für Physikalische Chemie* **1982**, *133*, 93-98.

58. Tesakova, M. V., Semeikin, A.S. & Parfenyuk, V.I. , Electrochemical Properties and Antioxidant Activity of Tetraphenylporphyrin Derivatives. *Russ. J. Electrochem.* **2015**, *51*, 686-692.

59. Yeh, T.-F.; Chan, F.-F.; Hsieh, C.-T.; Teng, H., Graphite Oxide with Different Oxygenated Levels for Hydrogen and Oxygen Production from Water under Illumination: The Band Positions of Graphite Oxide. *J. Phys. Chem. C* **2011**, *115*, 22587-22597.

60. Aydin, M.; Akins, D. L., Geometric and Electronic Properties of Porphyrin and Its Derivatives. In *Applications of Molecular Spectroscopy to Current Research in the Chemical and Biological Sciences*, Stauffer, M. T., Ed. InTech: Rijeka, 2016; p Ch. 10.